



**Continuous flow microfluidics for colloidal particle assembly
on porous substrates**

Journal:	<i>Soft Matter</i>
Manuscript ID	SM-ART-10-2022-001414.R1
Article Type:	Paper
Date Submitted by the Author:	28-Feb-2023
Complete List of Authors:	Lochab, Varun; The Ohio State University, Mechanical & Aerospace Engineering Ewim, Daniel; The Ohio State University, Mechanical & Aerospace Engineering Prakash, Shaurya; The Ohio State University, Department of Mechanical Engineering

ARTICLE

Continuous flow microfluidics for colloidal particle assembly on porous substrates

Received 00th January 20xx,
Accepted 00th January 20xx

DOI: 10.1039/x0xx00000x

Varun Lochab^a, E. Daniel Ewim^a, and Shaurya Prakash^{a*}

Self-assembly of colloidal particles for 'bottom-up' fabrication of various patterns and structures is critical for a range of applications including, but not limited to, energy migration, material science, biomimetics, and biosensing. Multiple self-assembly techniques, such as substrate templating — via topological or chemical patterning — and solvent evaporation were discussed in our previous papers and have been developed for the deposition of patterned self-assembled structures, such as bands of colloidal particles, on various substrates. While the templating techniques are limited due to the requirement of pattern-specific, prior substrate engineering to fabricate the desired structure, solvent evaporation requires longer assembly times and precise control over environmental conditions. In this paper, a template-free, continuous flow process, which is facilitated by continuous solvent drainage through porous substrates, is demonstrated for the self-assembly of colloidal particles into high-aspect ratio ($>10^3$, length to width) structures, such as linear arrays or grid structures. Colloidal particles were assembled both on polymeric and metallic porous membranes, with assembly times of $\sim 10^{-2}$ seconds per unit structure.

Introduction

Assembled colloidal particles (diameter $\varnothing = 0.1 - 1 \mu\text{m}$) have extensive applications, for example, light or energy harvesting and optoelectronics¹⁻⁴, biomimetic materials with specific reflection or wetting properties^{5, 6}, plasmonic resonators used in biological detection^{7, 8}, or flexible lasers⁹. In the past, colloidal particle assemblies with macroscopic properties and functions distinct from individual particles have relied on self-assembly methods^{10, 11}. In nature, self-assembly results in the hierarchical organization of interconnected components to generate complex structures and systems¹², albeit at a kinetically slower pace than human-engineered processes due to equilibrium thermodynamics¹³. For realizing rapid and large-scale bottom-up manufacturing, external forces using electric^{14, 15}, magnetic, or acoustic fields¹⁶ or directing self-assembly by substrate templating^{17, 18} have been proposed for overcoming the limitations of thermodynamically driven self-assembly processes. Nonetheless, the addition of these external stimuli can lead to higher defect densities^{19, 20} and requires significant auxiliary equipment to assemble colloidal particles.

Specifically, several techniques such as substrate templating *via* topological²¹ or chemical patterning²²⁻²⁴, convective self-assembly (CSA)^{25, 26}, or pre-assembly at the air-water interface²⁷ have also been demonstrated for directed self-assembly of colloidal particles. Non-convective processes such as those using electrostatic nanodroplet autofocusing have also been reported²⁸. However, both topological and chemical patterning requires substrate engineering prior to particle assembly while state-of-the-art CSA methods^{25, 26} for assembling band patterns on hydrophilic surfaces through controlled

evaporation of solvent require deposition periods on the order of 10 s or more^{26, 29}. Therefore, rapid and scalable fabrication of structures with at least one dimension at $O(\text{mm})$ from nanoscale and colloidal materials remains a significant technical challenge. By contrast, we have recently shown³⁰⁻³⁴ that colloidal particles aggregate and form stream-wise bands *inside* a microchannel under combined electrokinetic and Poiseuille flow, where bands have been shown to extend beyond the microchannel outlet for a few 100 μm . Past results show that band formation occurs over a minimum threshold of applied pressure gradient for a given electric field. Additionally, past work for particle migration and formation of bands within the channel have evaluated dependence of band formation on particle size and concentration, shear rate (controlled as a volumetric flow rate), electric field, fluid properties, and microchannel wall ζ -potential^{31, 33-35}. However, all past work has been limited to formation of bands *within* the microchannel with no reports on extracting these bands from the microchannel.

In this paper, we build on these recent discoveries by our team^{33, 34} and others^{30, 31, 35} that continuous flow with combined electrokinetic and Poiseuille flow can be used to form particle bands. Therefore, here a proof-of-concept, template-free process for rapid assembly of colloidal particles to high-aspect-ratio (*HAR*) structures (defined here as the length (*L*) to width (*W*) ratio due to the geometry of the assembled colloidal particles; $HAR (=L/W) > 10^3$) was demonstrated on both polymeric (polycarbonate, track-etched nanocapillary array membranes or (NCAM)^{36, 37} and metallic (silver) porous substrates.

Here, we report, the fastest time scales achieved for assembling these *HAR* structures organized as strips or bands of particles are $\sim 10^{-2}$ seconds on NCAMs, making the process more than 100-fold

^a Department of Mechanical and Aerospace Engineering, The Ohio State University, Columbus, 43210, OH.

*Corresponding Author: prakash.31@osu.edu

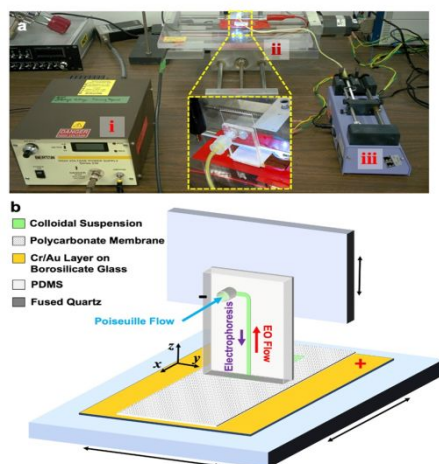


Figure 1: Experimental set-up. (a) Digital image of the set-up, where (i) is a high voltage supply, (ii) is an Arduino-controlled device set-up, and (iii) is a syringe pump for controlling fluid flow. Inset shows zoomed image of the microchannel print head. (b) Shows the schematic of device arrangement on the stage. Double-sided arrows show potential translation of the Arduino-controlled stage.

faster than other comparable processes^{25, 26, 29}. The essential parameters governing the assembly of colloidal particles to a substrate outside the microchannel from a microfluidic nozzle (referred to as the printing process in this work) are reported along with quantification of these printed structures for the observable characteristics like pitch and width of bands. Furthermore, parameters for assembly of dielectric colloidal particles organized as distinct bands on silver porous substrates was also evaluated with the chemical mapping of assembled structures. Therefore, the purpose of this paper is to demonstrate use of continuous microfluidics with combined electrokinetic and shear flow to assemble colloidal particles as distinct bands on porous substrates.

Materials and Methods

Fabrication. A microchannel-based print head (Figure 1), with a rectangular cross-section poly(dimethyl) siloxane (PDMS) microchannel was bonded to a fused silica microscope slide (50.8 mm × 25.4 mm × 1.0 mm, Esco Optics, Inc.). The PDMS microchannel was fabricated using a previously reported soft lithography process³⁸⁻⁴⁰. Briefly, photoresist (PR; SU-8 2025, MicroChem Corp., Newton, MA) was spin-coated (2150 rpm, 60 s) on a clean silicon (Si) wafer³⁴. Next, the spin-coated wafer was baked at 65°C for 5 minutes, and subsequently at 90°C for 10 minutes for evaporating the remaining solvent in the PR film. A transparency (10,000 dpi) photomask was employed for flood exposure (320-450 nm) with a total dose of 240 mJ/cm². Following the flood exposure, the wafer was again baked at 65°C for 3 minutes and then at 90°C for 10 minutes. Subsequently, the Si wafer with PR was developed for 7 minutes in SU-8 developer followed by a hard bake at 200°C for 15 minutes to yield a mould for the microchannel. Trichlorosilane was used to silanize the mold³⁸. Next, the 10:1 ratio of PDMS monomer and the curing agent respectively were mixed, and then

degassed for 1 hour in a vacuum desiccator. The degassed mixture was poured on the SU-8 mould, and the mould-PDMS assembly was cured for 4 hours at 70°C. The PDMS monoliths containing microchannels were gently peeled off the mould and a 3 mm hole was punched using a biopsy punch (Integra Miltex) for the fluid port. The PDMS microchannel was bonded microscope slides by exposing both the glass and PDMS to oxygen plasma at 45 W RF power and 280 mTorr pressure for 40 s to yield the PDMS microchannel-silica assembly³⁸. The bonding alignment between the PDMS microchannels and the glass slides was manually adjusted with a ~ 6 mm microchannel overhang from the edge of microscopic slides. The over-hang was then cut off manually from the edge of the glass using a razor blade to produce a rectangular cross-section microchannel outlet for the print head. The final microchannel dimensions were $\approx 3.4 \pm 0.1$ cm [L , length] × 340 μ m [W , width] × 35 μ m [H , height].

Printing Substrates and Particles. Polycarbonate track-etched (PCTE) nanocapillary array membranes (NCAMs)⁴¹ with ($\varnothing_{\text{capillary}} \approx 220$ nm) from GE Water & Process Technologies and nanoporous silver membranes (Fisher Scientific) were used as the porous substrates for the self-assembly of colloidal particles. Colloidal suspensions of yellow-green carboxylate-terminated fluorescent polystyrene (PS) particles with diameter 490 ± 15 nm (F8813, ThermoFisher Scientific, Lot Number 1934412245) with particle fraction (PF) 0.33% (w/v) were prepared in a sodium tetraborate buffer, Na₂B₄O₇·10H₂O (GFS Chemicals, ACS grade) at 1 mM (pH 9 ± 0.10) as reported previously^{33, 34}.

Experimental Set-up and Device Operation. An Arduino-controlled stage⁴², (Figure 1a) provided the printhead (Figure 1a, 1b) using Bertan High Voltage Power Supply, Series 230. To provide electrical contacts, a stainless-steel wire electrode (diameter ~ 0.60 mm) was inserted into the inlet reservoir while a layer of Cr/Au (4 nm/25 nm) was evaporated (CHA Solution System E-Gun Evaporator) on a microscope glass slide (75 mm × 50 mm, Fisherbrand™) placed under the printing substrate. For printing of colloidal particle structures, the stage was translated with velocity, $\mathbf{u}_s = \langle -0.63, 0, 0 \rangle$ mm/s, where boldface represents a vector with three components in x , y , and z respectively (Figure 1b), while the microchannel was fixed at a height (in z) of $\sim 190 \mu\text{m} \pm 60 \mu\text{m}$ from the top surface of porous substrate. Each printing experiment was carried out for 20 s to extract the pre-formed bands, which occur in the microchannels for the combined Poiseuille and electrokinetic flows reported here and take approximately 90 s to form within the microchannels^{30, 31, 34, 35}. Therefore, all printing evaluation was initiated after 90 s to ensure band formation within the microchannels. The use of a metallic substrate in porous silver eliminated the need for a secondary electrical connection as was used for the NCAMs. The printing yielded structures > 1 cm length (in x , Figure 1b) demonstrating the use of rapidly printing structures with continuous flow microfluidics. The Poiseuille flow was controlled by a programmable syringe pump (PicoPlus, Harvard Apparatus).

Imaging. A Nikon Eclipse Ti inverted microscope with Nikon Intensilight C-HGFI mercury lamp for illumination was used for imaging printed structures composed of fluorescent particles at either 4X or 10X magnification, while scanning electron microscopy

(SEM) was performed using Hitachi S-3000H instrument with an accelerating voltage of 5 kV.

Results and Discussion

Continuous flow printing. The continuous flow set-up was used to extract the pre-formed bands onto porous substrates, which facilitated drainage of the excess liquid leaving the particle bands on the substrates. Figure 2 shows a representative image of bands printed onto the NCAMs at a volumetric flow rate, $Q = 5 \mu\text{L}/\text{min}$ and an electric field, $E = -35 \text{ V}/\text{cm}$. The negative sign on E indicates that the Poiseuille flow and the electroosmotic flow are in opposite direction, which is a requirement for band formation within the microfluidic channel as reported previously^{33, 34}. Moreover, the relative direction of the two flows is shown schematically in Fig. 1.



Figure 2: Representative image of polystyrene (PS) particle bands printed on NCAMs. The printing was done at an applied electric field strength of $-35 \text{ V}/\text{cm}$ and a volumetric flow rate of $5 \mu\text{L}/\text{min}$. The pressure difference driving the Poiseuille flow and the electric field are in opposite directions. Nominal diameter of PS particles was 490 nm . NCAMs present a pore diameter of 220 nm to permit excess fluid drainage.

Observations of the printed bands indicate that the printed bands were high-aspect ratio ($\sim O(10^4)$). The number of bands observed is a function of the flow rate (i.e., shear rate from the Poiseuille flow) and the applied electric field. For the results reported here, the total number of bands was observed to vary between 10 to 30. Figure 2 shows approximately 26 bands in the field of view ($\sim 830 \mu\text{m} \times 630 \mu\text{m}$). Moreover, these bands display lengths $\sim 5 \text{ mm}$ or more post exit from the microchannel. Notably, the band length and several characteristics match in-channel bands when compared against previous results^{30, 31, 34}.

In order to evaluate the effect of volumetric flow rate on printing, post-banding within the microchannels, three distinct flow conditions were tested. The choice of volumetric flow rate at a fixed electric field is important as recent discoveries have shown that shear rate is an important parameter in these flows³⁵.

Table 1: Band characteristics (mean \pm S.D.) at three flow rates for a fixed electric field. Each test condition was repeated three times to obtain uncertainty in the printing process.

Table 1 summarizes width and pitch (i.e., the separation between bands) for the linear array of bands assembled at three different flow rates for known conditions where pre-assembly of colloidal particles within the microchannels is known³⁴. As seen in Table 1, with increasing flow rate both width and pitch were noted to decrease. Furthermore, when compared against previous reports of in-channel bands formation, the PS particle bands printed on NCAMs are significantly wider (for example, $\sim 2\text{X}$ wider with $\sim 3\text{X}$ increased pitch at $1 \mu\text{L}/\text{min}$), suggesting that during the printing formation as the

liquid drains convective dispersion may lead to band-spreading. The exact mechanisms of this convective dispersion and optimal combined flow conditions are a study in itself and therefore beyond the scope of this present work, where the purpose is to demonstrate

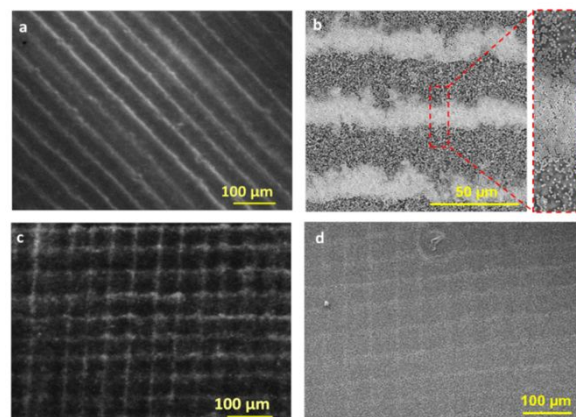


Figure 3: Demonstration of printing different structures. All printing at $Q = 1 \mu\text{L}/\text{min}$ and $E = -35 \text{ V}/\text{cm}$. (a) Linear array of bands printed at 45° angle to the horizontal. (b) Scanning electron microscopy (SEM) shows detailed structure of bands with unbanding particles in-between the bands. The inset shows further detail on the in-band particle structures. Scale bar is $30 \mu\text{m}$. (c) A 2D printed by overlaying two linear arrays printed orthogonally. (d) SEM micrograph of the 2D pattern.

a proof-of-concept method for continuous flow extraction of pre-formed particle assemblies. Nonetheless, the ratio of the pitch of assembled bands and stage velocity suggest that each band is printed or assembled at the substrate within $\sim 0.07 \text{ s}$, which is ~ 100 times faster than convective self-assembly using solvent evaporation that produces stripe patterns with a deposition period for each stripe on the order of $\sim 10 \text{ s}$ ^{26, 29}.

Printing different structures. Figure 3a shows the bands at $\sim 45^\circ$ from the horizontal can be obtained by the changing the orientation of the substrate with respect to x (Figure 1b) prior to printing assembly process with the representative image taken at $Q = 1 \mu\text{L}/\text{min}$ and $E = -35 \text{ V}/\text{cm}$. Figure 3b shows an SEM image of the self-assembled particles in the bands, with some particles observed in-between bands (Figure 3b) too. A two-dimensional (2D) structure was also printed (Figure 3c) by first printing along one direction on the substrate, and then the orientation of the substrate by rotated by $\sim 90^\circ$ with respect to x (Figure 1b). Therefore, manipulating stage control with respect to the continuous flow printing potentially provides an externally controlled method to build more complex structures. Figure 3d shows the SEMs of the 2D structure.

Flow Conditions	Width (μm)	Pitch (μm)
$Q = 1 \mu\text{L}/\text{min};$ $\Delta V_{12}/L = -35 \text{ V}/\text{cm}$	17.5 ± 9.7	44.6 ± 12.4
$Q = 3 \mu\text{L}/\text{min};$ $\Delta V_{12}/L = -35 \text{ V}/\text{cm}$	15.6 ± 4.7	41.6 ± 9.5
$Q = 5 \mu\text{L}/\text{min};$ $\Delta V_{12}/L = -35 \text{ V}/\text{cm}$	11.9 ± 5.2	25.0 ± 5.7

Printing on metallic substrate. Printing dielectric particles on silver substrate provided a new demonstration of using continuous flow microfluidic printing with pre-formed structures to rapidly make metal-dielectric interfaces. It must be noted bands could be printed only for the $Q = 5 \mu\text{L}/\text{min}$ flow rate. It is worth noting that change in flow conditions, electric fields, substrates, buffer ionic strength, and particle sizes has previously been shown to affect the exact conditions under which bands form^{30, 34}.

For further validation beyond visual confirmation, chemical imaging using a Thermo-Fisher Fourier Transform Infrared (FTIR) microscope was also conducted. Figure 4a shows the printed bands with the dotted box forming the region for Fig. 4b. The FTIR microscope records the chemical spectra (Fig. 4c) and allows the image for the different spectra to be overlaid as a chemical image that shows PS particles (in red and green) compared to the Ag background (blue). The comparison against standard PS FTIR confirms the visual mapping of the particle bands.

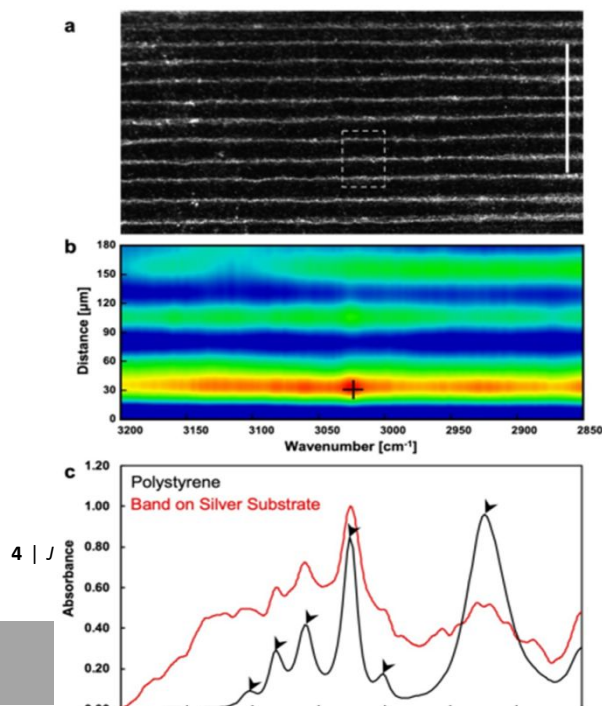


Table 2: Summary of the calculated magnitudes of essential non-dimensional parameters.

Non-dimensional Parameter	Calculated Value
Reynolds Number, Re	$\sim 10^{-1}$ (within capillary bridge)
Capillary Number, Ca	$\sim 10^{-5}$
Bond Number, Bo	$\sim 10^{-5}$
Electrocapillary number, Ca_E	$\sim 10^{-5}$

Analysis of band printing. The printing of pre-formed bands with a continuous flow configuration presents a complex problem. To illustrate this complexity consider that printing occurs through a rectangular cross-section microchannel with an impinging jet to a porous substrate with the fluid containing locally concentrated particles, organized to band-structures, in a combined Poiseuille and electrokinetic flow. It is also noteworthy that at present the theory for explaining band formation within microchannels diverges significantly from experiments⁴³ and no consensus model exists³³. During the printing process, a three-dimensional capillary bridge was maintained by continuous flow of the colloidal suspension from the microchannel to the porous substrate. Given the knowledge gaps in state-of-art for the models for formation and printing of these bands, we present a first-order scaling analysis using well-known but simplified governing equations to estimate relevant non-dimensional parameters to gain insight to the physical printing process.

The essential non-dimensional parameters that can be evaluated for the band-printing problem would be: (i) the Reynolds number, Re in the capillary bridge that provides a comparison between the inertial to viscous forces during the transfer of the fluid and particles to the porous substrate; (ii) the capillary number, Ca for the NCAMs (model porous substrate for analysis) as the fluids drains from the NCAMs and provides an estimate of the viscous forces against the surface-tension induced capillary forces; (iii) The bond number, Bo to evaluate if the fluid drainage in the vertical direction through the porous substrates introduces gravity as an important parameter during printing; and (iv) the electrocapillary number⁴⁴, Ca_E to consider the role of electric field in contrast to the pressure gradients. Table 2 presents a summary of these four non-dimensional parameters assuming, that the printing process occurs at steady state, the fluid remains incompressible, and despite band formation, the colloidal suspension is dilute and colloidal particles ($PF = 0.33 \text{ \% w/v}$) do not disturb fluid velocity and travel along the fluid in the capillary bridge as organized bands. Moreover, we note,

the motion of stage shears the capillary bridge and the magnitude of stage velocity, $u_s \sim u$, is the velocity component in x . Moreover, the scales for changes in (x, y, z) , are given by (r_x, r_y, r_z) , where r_x is the width of the capillary bridge along x , r_y is the width of the capillary bridge along y , and r_z is the gap between microchannel outlet and the substrate. We know from experimental observations that the height of the capillary bridge i.e., gap between porous substrate and microchannel outlet, $r_z \ll r_x, r_y$ as $r_x, r_y \sim O(1 \text{ mm})$ and $r_z \sim O(0.1 \text{ mm})$. Since, $r_z/r_x \ll 1$ and $r_y/r_x \sim 1$, then, $w \ll u, v$. Moreover, as the fluid drains through the NCAMs, the applied pressure gradient for Poiseuille flow for the microchannel is not the primary draining pressure but the capillary pressure $p \sim \sigma/r_z$ with σ being the surface tension of water is the dominant pressure. All fluid properties were for water at standard room temperature and pressure.

From Table 2, it is evident that post-exit from the microchannel, printing is dominated due to the surface tension of the fluid with $Ca \sim Bo \sim Ca_E \ll 1$ for the weakly inertial flows ($Re \sim 0.1$ in the capillary bridge). The calculated values for Ca , Bo , and Ca_E along with the size of the capillary bridge suggests that the capillary bridge can be approximated as a slender bridge and for such bridges, effects of gravity and electric field on bridge-bending can be neglected⁴⁴. Consequently, it is expected that the capillary bridge would retain its observed shape during the printing process⁴⁵⁻⁴⁷. It is noteworthy that for the weakly inertial flows considered here, Ca and Ca_E scale linearly with the velocity in the x -direction (i.e., $u_s \sim u$). Therefore, to alter the printing dynamics, an increase in u_s by at least an order of magnitude or more is needed to impact the capillarity and electrocapillarity of the fluid bridge.

Summary and Conclusions

Past work has demonstrated that colloidal particles with diameters $< 1 \mu\text{m}$ can be assembled to distinct bands *within* a microchannel for certain combinations of oppositely directed electric potential and pressure gradients. Using these conditions, a continuous particle band-printing system was developed and characterized for the extraction of model polystyrene particles on both dielectric substrates such as the nanocapillary array membranes or on conducting substrates such as a porous silver substrate. The ability to print sub-micron colloidal particles may be useful in applications such as biosensing⁴⁸ and others as articulated in the introduction. The results show that the printed bands are stable structures with the printing process dominated by the removal of excess fluid, suggesting a role for the surface tension of the liquid during the printing process.

Author Contributions

SP: Designed, planned, and conceived the experiments. VL: Conducted the experiments and analysis. DE: Assisted with analysis. All authors contributed to manuscript development and writing.

Conflicts of interest

There are no conflicts to declare.

Acknowledgements

The US Army Research Office funded this work through grant number W911NF-16-0278 and W911-NF-1-0144. We thank the Campus Microscopy and Imaging Facility, The Ohio State University. This facility is supported in part by grant P30 CA016058, National Cancer Institute, Bethesda, MD. We also thank the staff of Nanotech West for helping with device fabrication and characterization. We thank Professor Minami Yoda (Georgia Institute of Technology) and Professor A.T. Conlisk (The Ohio State University) for their time devoted to many a conversation relevant to the topics of this paper.

References

1. B. Amir Parviz, D. Ryan and G. M. Whitesides, *IEEE Transactions on Advanced Packaging*, 2003, **26**, 233-241.
2. J. F. Galisteo-Lopez, M. Ibsate, R. Sapienza, L. S. Froufe-Pérez, A. Blanco and C. López, *Advanced Materials*, 2011, **23**, 30-69.
3. Z. Hanbin and S. Ravaine, *Crystals*, 2016, **6**, 54.
4. D. J. Hynek, J. V. Pondick and J. J. Cha, *APL Materials*, 2019, **7**, 030902.
5. W.-L. Min, B. Jiang and P. Jiang, *Advanced Materials*, 2008, **20**, 3914-3918.
6. T. Kraus, D. Brodoceanu, N. Pazos-Perez and A. Fery, *Advanced Functional Materials*, 2013, 4529.
7. J. N. Anker, W. P. Hall, O. Lyandres, N. C. Shah, J. Zhao and R. P. Van Duyne, *Nature Materials*, 2008, **7**, 442-453.
8. P. C. Jon, A. D. Jon, Z. Jing and P. V. D. Richard, *Accounts of Chemical Research*, 2008, **41**, 1653-1661.
9. S. Furumi, H. Fudouzi, H. T. Miyazaki and Y. Sakka, *Advanced Materials*, 2007, **19**, 2067-2072.
10. M. A. Boles, M. Engel and D. V. Talapin, *Chemical reviews*, 2016, **116**, 11220-11289.
11. Z. Xu, L. Wang, F. Fang, Y. Fu and Z. Yin, *Current Nanoscience*, 2016, **12**, 725-746.
12. H. Kuhn and A. Ulman, in *Thin Films*, ed. A. Ulman, Elsevier, 1995, vol. 20, pp. 1-7.
13. S. Hormoz and M. P. Brenner, *Proc Natl Acad Sci U S A*, 2011, **108**, 5193-5198.
14. E. V. Yakovlev, K. A. Komarov, K. I. Zaytsev, N. P. Kryuchkov, K. I. Koshelev, A. K. Zotov, D. A. Shelestov, V. L. Tolstoguzov, V. N. Kurlov, A. V. Ivlev and S. O. Yurchenko, *Scientific reports*, 2017, **7**.
15. W. Liu, J. Shao, Y. Jia, Y. Tao, Y. Ding, H. Jiang and Y. Ren, *Soft Matter*, 2015, **11**, 8105-8112.
16. N. A. Sapozetova, N. A. Martynova, K. S. Napolskii, A. A. Eliseev, A. V. Lukashin, I. V. Kolesnik, D. I. Petukhov, S. E. Kushnir, A. V. Vassilieva, S. V. Grigoriev, N. A. Grigoryeva, A. A. Mistonov, D. V. Byelov and Y. D. Tret'yakov, *Phys. Solid State Physics of the Solid State*, 2011, **53**, 1126-1130.
17. Y. Yadong, L. Yu, B. Gates and X. Younan, *Journal of the American Chemical Society*, 2001, **123**.
18. N. Vogel, M. Retsch, C. A. Fustin, A. Del Campo and U. Jonas, *Chemical Reviews*, 2015, **115**, 6265-6311.
19. M. Grzelczak, J. Vermant, E. M. Furst and L. M. Liz-Marzán, *ACS Nano*, 2010, **4**, 3591-3605.
20. R. van Dommelen, P. Fanzio and L. Sasso, *Advances in Colloid and Interface Science*, 2018, **251**, 97-114.
21. N. Vogel, L. de Viguerie, U. Jonas, C. K. Weiss and K. Landfester, *Advanced Functional Materials*, 2011, **21**, 3064-3073.
22. I. Lee, H. Zheng, M. F. Rubner and P. T. Hammond, *Advanced Materials*, 2002, **14**, 572.

23. J. Aizenberg, P. V. Braun and P. Wiltzius, *Physical Review Letters*, 2000, **84**, 2997-3000.
24. Q. Guo, C. Arnoux and R. E. Palmer, *Langmuir*, 2001, **17**, 7150-7155.
25. S. Watanabe, K. Inukai, S. Mizuta and M. T. Miyahara, *Langmuir*, 2009, **25**, 7287-7295.
26. Y. Mino, S. Watanabe and M. T. Miyahara, *ACS applied materials & interfaces*, 2012, **4**, 3184-3190.
27. M. Retsch, K.-H. Dostert, S. K. Nett, N. Vogel, J. S. Gutmann and U. Jonas, *Soft Matter*, 2010, **6**, 2403.
28. P. Galliker, J. Schneider, H. Eghlidi, S. Kress, V. Sandoghar and D. Poulikakos, *Nature Communications*, 2012, **3**.
29. Y. Mino, S. Watanabe and M. T. Miyahara, *Langmuir*, 2011, **27**, 5290-5295.
30. A. Yee and M. Yoda, *Microfluidics and Nanofluidics*, 2018, **22**, 1-12.
31. N. Cevheri and M. Yoda, *Lab on a Chip*, 2014, **14**, 1391-1394.
32. S. Prakash and V. Lochab, *Bulletin of the American Physical Society*, 2020, **65**.
33. V. Lochab and S. Prakash, *Soft matter*, 2021, **17**, 611-620.
34. V. Lochab, A. Yee, M. Yoda, A. Conlisk and S. Prakash, *Microfluidics and Nanofluidics*, 2019, **23**, 1-13.
35. A. J. Yee and M. Yoda, *Electrophoresis*, 2021, **42**, 2215-2222.
36. V. V. Swaminathan, L. R. Gibson, M. Pinti, S. Prakash, P. W. Bohn and M. A. Shannon, *Journal of Nanoparticle Research*, 2012, **14**, 951.
37. S. Prakash, A. Piruska, E. N. Gatimu, P. W. Bohn, J. V. Sweedler and M. A. Shannon, *IEEE Sensors Journal*, 2008, **8**, 441-450.
38. D. C. Duffy, J. C. McDonald, O. J. Schueller and G. M. Whitesides, *Analytical chemistry*, 1998, **70**, 4974-4984.
39. D. Qin, Y. Xia and G. M. Whitesides, *Nature protocols*, 2010, **5**, 491.
40. E. Akbari, G. B. Szychalski, K. K. Rangharajan, S. Prakash and J. W. Song, *Lab on a Chip*, 2018, **18**, 1084-1093.
41. K. K. Rangharajan, M. Fuest, A. T. Conlisk and S. Prakash, *Microfluidics and Nanofluidics*, 2016, **20**.
42. S. Prakash, M. P. Karnes, E. K. Sequin, J. D. West, C. L. Hitchcock, S. D. Nichols, M. Bloomston, S. R. Abdel-Misih, C. R. Schmidt, E. W. Martin, S. P. Pivoski and V. V. Subramaniam, *Physiological Measurement*, 2015, **36**, 315-328.
43. A. S. Khair and J. K. Kabarowski, *Physical Review Fluids*, 2020, **5**.
44. A. G. Marin and D. Lohse, *Physics of Fluids*, 2010, **22**.
45. S. Dodds, M. S. Carvalho and S. Kumar, *Journal of fluid mechanics*, 2012, **707**, 521-540.
46. S. Kumar, S. Dodds and M. Carvalho, 2012.
47. S. Kumar, *Annual Review of Fluid Mechanics*, 2015, **47**, 67-94.
48. M. Oliverio, S. Perotto, G. C. Messina, L. Lovato and F. D. Angelis, *ACS applied materials & interfaces*, 2017, **9**, 29394-29411.